FERMILAB-CONF-14-265-E
CDF Note 11104
D0 Note 6443

Combined CDF and D0 Constraints on Models for the Higgs Boson with Exotic Spin and Parity

The TEVNPH Working Group*

for the CDF and D0 Collaborations

September 10, 2014

We combine the results from the CDF and D0 tests of models of the Higgs Boson with exotic spin and parity. The data set analyzed by the CDF and D0 Collaborations corresponds to approximately 10 fb^{-1} per experiment of $p\bar{p}$ collision data collected at the Fermilab Tevatron at $\sqrt{s} = 1.96$ TeV. Two models of exotic Higgs boson production are considered: a pseudoscalar Higgs boson with $J^P = 0^-$ and a graviton-like state with $J^P = 2^+$. In these models, the kinematics of Higgs boson production in association with a vector boson are very different from those predicted for the Standard Model Higgs boson, which has $J^P = 0^+$. Both the CDF and D0 Collaborations have re-optimized their searches for $WH \to \ell\nu b\bar{b}$, $ZH \to \ell^+\ell^- b\bar{b}$, and $WH + ZH \to \not{E}_T b\bar{b}$ to test the exotic Higgs boson models. Upper limits at 95% CL on the production rate of an exotic Higgs boson, X, times the decay branching ratio $Br(X \to b\bar{b})$ are set at 0.36 times that predicted for the SM Higgs boson for the 2^+ hypothesis, and 0.36 times that predicted for the SM Higgs boson for the 0^- hypothesis. If the production rate times the $(X \to b\bar{b})$ branching ratio of the exotic particle is the same as that predicted for the SM Higgs boson, then the exotic models are excluded with significances of 4.9 s.d. and 5.0 s.d. for the 2^+ and 0^- models, respectively.

Preliminary Results

* The Tevatron New-Phenomena and Higgs Working Group can be contacted at TEVNPHWG@fnal.gov. More information can be found at http://tevnphwg.fnal.gov/.

I. INTRODUCTION

The Higgs boson, discovered by the ATLAS [1] and CMS [2, 3] Collaborations in 2012 using data produced by the Large Hadron Collider (LHC) at CERN, provides an excellent system for studying the mechanism of electroweak symmetry breaking, and may provide a window to physics beyond the Standard Model (SM). The properties of the boson discovered at CERN are under intense study – its mass [3, 4], its couplings to other SM particles via its production and decay rates [3, 5, 6], and its spin and parity quantum numbers [7, 8]. Within the uncertainties the observed particle has the properties of the SM Higgs boson.

At the Tevatron, a broad suite of searches for the SM Higgs boson resulted in an expected sensitivity of 1.9 standard deviations (s.d.); an excess of Higgs boson candidate events over the background predictions resulted in an observed significance of 3.0 s.d. [6]. In this study, the production rate in the associated production modes WH and ZH times the decay branching ratio $H \to b\bar{b}$ was also measured. Tevatron data also constrain the production rates for $gg \to H$, $t\bar{t}H$, and vector-boson fusion (VBF), as well as the decays $H \to W^+W^-$, $H \to \tau^+\tau^-$, $H \to ZZ$, and $H \to \gamma\gamma$.

Recently, it was proposed to use the associated production modes WX and ZX with the decay $X \to b\bar{b}$ to test the spin and parity characteristics of an exotic state, X [10]. This proposal makes use of the spin and parity models in Ref. [11], and the fact that the product of the matrix element and phase space predictions for different J^P assignments differ by two or more powers of $\beta = 2p/\sqrt{s}$, where p is the momentum of the Higgs boson in the VH ($V = W$ or Z) reference frame, and $\sqrt{s}$ is the total energy of the VH system in its rest frame [11]. For the pseudoscalar model ($J^P = 0^-$) proposed, the factor is β^3, and for the graviton-like boson ($J^P = 2^+$), the factor is β^5, whereas for the SM assignment, $J^P = 0^+$, the factor is β. These factors alter the kinematic distributions of the observable decay products of the vector boson and the Higgs-like boson X. The variable most strongly affected is the invariant mass of the VX system, which has a much higher average value in the 0^- hypothesis than the SM 0^+ case, and higher still in the 2^+ hypothesis. Not all possible $J^P = 2^+$ bosons share this feature however, and Ref. [11] enumerates several that have no additional factor of β, leaving them untestable at the Tevatron using the kinematic method proposed in Ref. [10].

The ATLAS and CMS Collaborations have examined the possibility that the H boson has $J^P = 0^-$ or $J^P = 2^+$ using its decays to $\gamma\gamma$, ZZ, and W^+W^- states [7–9]; however, the J^P character of Higgs bosons decaying to fermions has not yet been studied. The $J^P = 0^-$ hypothesis is excluded at the 97.8% and 99.95% CL by the ATLAS and CMS Collaborations, respectively, in the $H \to ZZ \to 4\ell$ decay mode. Likewise, the $J^P = 2^+$ hypothesis is excluded at the $\geq 99.9\%$ CL by the ATLAS Collaboration when combining all bosonic decay modes, and at the $\geq 97.7\%$ CL by the CMS Collaboration in the $H \to ZZ \to 4\ell$ decay mode (depending on the production processes and the quark mediated fraction of the production processes).

The particle observed at the LHC might not be the same particle for which evidence was found at the Tevatron [12]. The production and decay mechanisms are different, though the suite of measurements is consistent with that predicted by the SM Higgs boson. The CMS Collaboration has published strong evidence for decays of the Higgs boson to fermions [13]; the sensitivity is dominated by the $H \to \tau\tau$ final state, and both the ATLAS and CMS Collaborations have reported evidence in this final state [14, 15]. Both collaborations have also carried out searches in the bb final state [16, 17], though, as mentioned above, spin and parity tests have not yet been performed in these decay modes. Performing the tests proposed in Ref. [10] using Tevatron data provides a valuable check of the identity of the particle or particles responsible for the excess events seen at the Tevatron. In the case that 0^+ is favored, this test helps complete the picture provided by the Tevatron data in support of a SM-Higgs-like explanation for the data, while an outcome favoring one of the two exotic hypotheses would cast doubt on the presence of a single Higgs boson and provide strong motivation to test further the nature of the new particle(s).

II. GENERAL STRATEGY

Ref. [10] proposed using the M_{VX} distribution to test the two alternate J^P models against the SM Higgs boson hypothesis using Tevatron data. A high sensitivity was predicted assuming that the background in the search can be neglected. Predictions for the production cross sections and decay branching ratios are not available for the exotic models, and are model dependent [18]. If a search for a Higgs-like particle at the Tevatron could be conducted with minimal sculpting of kinematic distributions by the trigger and selection requirements, and if the resulting background

were small, then the properties of the selected sample of candidate events can be used to test for the spin and parity properties of the new particle. This is largely the case at the LHC, where the signal-to-background ratio in the $H \to ZZ \to \ell^+\ell^-\ell^+\ell^-$ exceeds 2:1 with minimal kinematic sculpting, and the five measurable angles provide strong constraints on the spin and parity of the Higgs boson. In the case of the Tevatron searches, however, due to the large SM background contributions and the necessity of using multivariate analysis (MVA) event selection techniques to select subsamples with a broad range of signal purity, the proposed strategy needs to be modified. CDF and D0 have taken different approaches to this modification, and have conducted tests of the proposed exotic models. CDF has adapted its MVA searches for the SM Higgs boson to test for the exotic Higgs bosons as possible new particles, either in addition to, or replacing, the SM Higgs boson [19]. D0 has selected low and high purity signal samples, using either the reconstructed dijet mass or the MVA used in SM Higgs boson search, depending on the channel in question. The mass of the VX system is then used to discriminate between the non-SM X and SM hypotheses [20]. While these analyses are based on their SM counterparts, they are optimized to distinguish the 0^- and the 2^+ hypotheses from the SM 0^+ hypothesis, and not for the observation of the 0^+ hypothesis; the analyses optimized to separate the 0^+ signal from the background are detailed in Ref [6] and references therein. The results of these differently-optimized searches are combined using the techniques described in Ref. [6]. These techniques have been modified to allow the possibility of two signals with different kinematic properties simultaneously present in the data.

III. SAMPLE SELECTIONS AND BACKGROUNDS

Event selections are similar for the corresponding CDF and D0 analyses, consisting typically of a preselection followed by the use of a multivariate analysis technique with a final discriminating variable to separate signal and background. In the case of D0, the $WH \to \ell\nu b\bar{b}$ [21], $ZH \to \nu\nu b\bar{b}$ [22] and $ZH \to \ell\ell b\bar{b}$ [23] analyses are used without any modification of the event selection.

For the case of $WH \to \ell\nu b\bar{b}$, an isolated lepton (ℓ = electron or muon) and two or three jets required, with one or more b-tagged jets, i.e., identified as containing a weakly-decaying b hadron. Selected events must also display a significant imbalance in transverse momentum (referred to as missing transverse energy or $\not\!\!E_T$). Events with more than one isolated lepton are rejected.

For the D0 $WH \to \ell\nu b\bar{b}$ analyses, the data are split by lepton flavor and jet multiplicity (two or three jet sub-channels), and by the output of the b-tagging algorithm applied to all selected jets in the event. As with other D0 analyses targeting the $H \to b\bar{b}$ decay, the $WH \to \ell\nu b\bar{b}$ analyses uses an MVA based b-tagging algorithm [24, 25] that exploits information on the track impact parameters, secondary vertices and event topology to discriminate between b and light jets. Four exclusive b-tagging categories, "one-tight-tag" (1TT), "two-loose-tag" (2LT), "two-medium-tag" (2MT), and "two-tight-tag" (2TT) are formed. Events with one b-tagged jet are categorized by the b-tagging discriminant output for a single jet. Events with more than one b-tagged jet are categorized by the average of the b-tagging discriminant outputs of the two jets with the highest discriminant outputs into the three two-tag categories. D0 achieves b-tagging identification efficiencies of $\approx 80\%$ ($\approx 50\%$) for true b-jets, for a mis-identification rate of $\approx 10\%$ ($\approx 0.5\%$). The outputs of boosted decision trees, trained separately for each sample are used as the final discriminating variables in the SM Higgs boson search.

For the CDF $WH \to \ell\nu b\bar{b}$ analyses, events are analyzed in only the two-jet category for this study. Events are classified into separate analysis categories based on the quality of the identified lepton. Separate categories are used for events with a high quality muon or central electron candidate, an isolated track, or a forward electron candidate. Within the lepton categories there are five b-tagging categories considered for two-jet events: two tight b tags (TT), one tight b tag and one loose b-tag (TL), two loose b-tags (LL), a single tight b-tag (T), and a single loose b tag (L). Only jets with $E_T < 200$ GeV are considered for b-tagging in CDF due to the fact that the Higgs-Optimized B Identification Tagger (HOBIT) [26] used here was trained on SM Higgs boson signal Monte Carlo (MC) events which did not contain sufficient quantities of jets with $E_T > 200$ GeV and thus does not perform well for these jets.

For the $ZH \to \nu\bar{\nu}b\bar{b}$ analyses, the selection is similar to the WH selection, except all events with isolated leptons are rejected and stronger multijet background suppression techniques are applied. Both the CDF and D0 analyses use a track-based missing transverse momentum calculation as a discriminant against false $\not\!\!E_T$. In addition both CDF and D0 utilize multivariate techniques, a boosted decision tree at D0 and a neural network at CDF, to further discriminate against the multijet background before b-tagging. There is a sizable fraction of the $WH \to \ell\nu b\bar{b}$ signal

in which the lepton is undetected that is selected in the $ZH \to \nu\bar{\nu}b\bar{b}$ samples, so these analyses are also referred to as $VH \to \not{E}_T b\bar{b}$. The CDF analysis uses three non-overlapping b-tag categories (TT, TL, and T), and two jet categories (two- or three-jet events) giving a total of six sub-channels. In the D0 analysis, exactly two jets are required and two exclusive categories, the medium (MT) and tight (TT), are defined using the sum of the b-tagging outputs for each of the two selected jets. In the SM Higgs boson search, CDF uses neural-network outputs for the final discriminating variables, while D0 uses boosted decision tree outputs.

The $ZH \to \ell^+\ell^- b\bar{b}$ analyses require two isolated leptons and at least two jets. D0's $ZH \to \ell^+\ell^- b\bar{b}$ analyses separate events into non-overlapping samples of events with either a single tight b-tag (ST) or a double tag (DT). CDF separates events into tight single tag (T), tight double tag (TT), tight-loose double tag (TL), and loose double tag (LL) samples. To increase signal acceptance D0 loosens the selection criteria for one of the leptons to include an isolated track not reconstructed in the muon detector ($\mu\mu_{trk}$) or an electron candidate from the inter-cryostat region of the D0 detector (ee_{ICR}). Combined with the dielectron (ee) and dimuon ($\mu\mu$) analyses, these provide four orthogonal analyses, each divided into two b-tagging categories. CDF uses neural networks to select loose dielectron and dimuon candidates. D0 applies a kinematic fit to optimize reconstruction, while CDF corrects jet energies for $\not{E}_T$ using a neural network approach. D0 uses random forests (RF) of decision trees to provide the final variables in the SM Higgs boson search. The first RF is designed to discriminate against $t\bar{t}$ events and divides events into $t\bar{t}$-enriched and $t\bar{t}$-depleted ST and DT regions. Only events in the $t\bar{t}$-depleted ST and DT regions are considered in this study. These regions contain $\approx 94\%$ of the SM signal. CDF utilizes a multi-layer discriminant based on neural networks where two discriminant functions are used to define three separate regions of the final discriminant function.

Both CDF and D0 see an increase in acceptance for the 2^+ and 0^- models in the $ZH \to \nu\bar{\nu}b\bar{b}$ analyses with respect to their SM Higgs counterparts. The factor is roughly 1.5 in the acceptance, and it is largely due to the exotic signal events more easily passing the trigger thresholds for $\not{E}_T$. The other two channels, $WH \to \ell\nu b\bar{b}$ and $ZH \to \ell^+\ell^- b\bar{b}$ do not benefit as much from the additional $\not{E}_T$ in these events, as they rely on the lepton triggers which are much more efficient than the $\not{E}_T$ triggers in the relevant kinematic regions.

SM and instrumental background processes are modeled using a mixture of MC and data-driven methods. In the CDF analyses, backgrounds from SM processes with electroweak gauge bosons or top quarks are modeled using PYTHIA [27], ALPGEN [28], MC@NLO [29], and HERWIG [30]. For D0, these backgrounds are modeled using PYTHIA, ALPGEN, and SINGLETOP [31], with PYTHIA providing parton-showering and hadronization for all the generators. Diboson (WW, WZ, ZZ) MC samples are normalized using the NLO calculations from MCFM [32]. For top-quark-pair production ($t\bar{t}$), we use a production cross section of 7.04 ± 0.49 pb [33], which is based on a top-quark mass of 173 GeV/c^2 [34] and MSTW 2008 PDFs [35]. The single-top-quark production cross section is taken to be 3.15 ± 0.31 pb [36]. For many analyses, the V+jet processes are normalized using the NNLO cross section calculations of Ref. [37], though in some cases data-driven techniques are used. Likewise, the normalization of the instrumental, multijet and, for the CDF searches, the V+heavy-flavor jet backgrounds are constrained from data samples where the expected signal-to-background ratio is several orders of magnitude smaller than in the search samples. For the D0 searches, the V+light-flavor is normalized to data in a control region, and the V+heavy-flavor normalization, relative to the V+light-flavor, is taken from MCFM. In addition, for the D0 searches, prior to b-tagging V+jets samples are compared to data and corrections applied to mitigate any discrepancies in kinematic distributions.

IV. SIGNAL PREDICTIONS

We normalize the Higgs boson signal predictions to the highest-order calculations available at the time of the studies. Our WH and ZH cross sections are from Ref. [38]. This calculation starts with the NLO calculation of V2HV [39] and includes NNLO QCD contributions [40], as well as one-loop electroweak corrections [41]. The cross sections used are listed in Table I.

In order to predict the kinematic distributions of Higgs boson signal events, CDF and D0 use the PYTHIA MC program, with CTEQ5L and CTEQ6L1 [42] leading-order (LO) parton distribution functions, respectively.

The $J^P = 0^-$ and $J^P = 2^+$ signal samples are generated using MADGRAPH 5 version 1.4.8.4 [43]; the exotic signal model components were provided by the authors of Ref. [10]. We have verified that $J^P = 0^+$ samples produced with MADGRAPH agree well with the SM PYTHIA simulations.

TABLE I: The production cross sections and decay branching fractions for the SM Higgs boson assumed for the combination.

m_H (GeV/c^2)	$\sigma_{gg\to H}$ (fb)	σ_{WH} (fb)	σ_{ZH} (fb)	σ_{VBF} (fb)	$\sigma_{t\bar{t}H}$ (fb)	$B(H\to bb)$ (%)
125	949.3	129.50	78.5	65.3	4.279	57.8

The Higgs boson decay branching ratio predictions used for this result are those of Refs. [44, 45]. In this calculation, the partial decay widths for all Higgs boson decays except to pairs of W and Z bosons are computed with HDECAY [46], and the W and Z pair decay widths are computed with PROPHECY4F [47]. The relevant decay branching ratios are listed in Table I. The uncertainties on the predicted branching ratios from uncertainties in m_b, m_c, and α_s are presented in Refs. [48, 49].

Tables II and III summarize, for CDF and D0 respectively, the channels over which the searches are performed. References to further details for each analysis are also given.

TABLE II: Luminosity and references for the different processes and final states ($\ell = e$ or μ) for the CDF analyses. The generic labels "2×" and "3×" refer to separations based on lepton categories.

Channel	Luminosity (fb^{-1})	Reference
$WH\to\ell\nu bb$ 2-jet channels 3×(TT,TL,T,LL,L)	9.45	[50]
$ZH\to\not{E}_T b\bar{b}$ (TT,TL,T)	9.45	[51]
$ZH\to\ell^+\ell^- b\bar{b}$ 2×(TT,TL,T,LL)	9.45	[52]

TABLE III: Luminosity and references for the different processes and final states ($\ell = e$ or μ) for the D0 analyses. The generic labels "2×" and "4×" refer to separations based on lepton categories.

Channel	Luminosity (fb^{-1})	Reference
$WH\to\ell\nu bb$ 2×(1TT,2LT,2MT,2TT,2,3 jet)	9.7	[21]
$ZH\to\nu\bar{\nu}b\bar{b}$ (MT,TT)	9.5	[22]
$ZH\to\ell^+\ell^- b\bar{b}$ 4×(ST,TT)	9.7	[23]

V. FINAL DISCRIMINANT VARIABLES

Because these searches are largely based on the searches for the SM Higgs boson but are re-purposed to test for the 0^- and 2^+ hypotheses, new final discriminants have been optimized in each channel. The possible presence of two Higgs-like particles guides the construction of appropriate discriminant variables; sensitivity to both the SM Higgs boson and the exotic Higgs boson are simultaneously desired.

For CDF, the discriminants are based on the MVA functions used in the searches for the SM Higgs boson, re-optimized for the exotic scenarios. In the $WX\to\ell\nu b\bar{b}$ channel, the discriminants are re-trained using either the 0^- or the 2^+ model as the signal, thus producing two discriminants, D_{0^-} and D_{2^+} for each sub-channel, for separating the 0^- signal or the 2^+ signal from the background. The discriminant used in the SM Higgs boson search is denoted here as D_{0^+}. Each discriminant is scaled so that its value is in the range [0,1]. In the 0^- search, if $D_{0^-} > 0.5$, then D_{0^-}

is used as the final discriminant, otherwise $D_{0^+}/2$ is used as the final discriminant, and similarly for the 2^+ searches. The list of variables used as inputs to the discriminants is similar to that used for the SM Higgs boson search. The SM Higgs boson search did not use the variable $M_{\ell\nu b\bar{b}}$ however, and it was not added for this analysis. Instead, H_T, which is the scalar sum of all of the transverse energies in the event, serves as a proxy.

In CDF's $VH \to \not{E}_T b\bar{b}$ search, a similar approach is taken, though the anti-QCD neural network has been re-trained using the exotic signals. The exotic-Higgs discriminant is chosen if its value exceeds 0.6, and otherwise the SM Higgs discriminant is used. The variables used as inputs to the discriminants are the same as those used in the SM Higgs boson search. The transverse mass of the $\not{E}_T b\bar{b}$ system was in the SM Higgs boson search input variable list and did not need to be added.

In CDF's $ZH \to \ell^+\ell^- b\bar{b}$ search, the neural network strategy already is a cascade of several neural networks applied in turn, and so only a new discriminant, trained to separate the exotic signal from the background but not to separate the exotic signal from the SM Higgs boson signal is applied.

D0 uses the mass of the VX system to discriminate between the different J^P signal hypotheses. For the $ZH \to \ell\ell b\bar{b}$ analysis the invariant mass of the two leptons and either the two highest b-tagged jets (DT) or the b-tagged jet and highest p_T non-tagged jet (ST) are used. For the $\ell\nu b\bar{b}$ and $\nu\nu b\bar{b}$ final states D0 uses the transverse mass, defined as $M_T^2 = (E_T^V + E_T^X)^2 - (\vec{p}_T^V + \vec{p}_T^X)^2$ where the transverse momenta of the Z and W bosons are $\vec{p}_T^Z = \not{E}_T$ and $\vec{p}_T^W = \not{E}_T + \vec{p}_T^\ell$. In the $WH \to \ell\nu b\bar{b}$ analyses the two jets can either be one b-tagged jet (1TT) and the highest p_T non-tagged jet, or the two b-tagged jets from any of the two b-tag categories (2LT, 2MT or 2TT). For the $ZH \to \nu\nu b\bar{b}$ analysis the two jets are from either the medium (MT) or tight (TT) b-tagging channels.

To further improve the discrimination between the signal and SM backgrounds, D0 uses the invariant mass M_{jj} of the dijet system in the $\ell\ell b\bar{b}$ and $\nu\nu b\bar{b}$ final states and the final multivariate analysis output of the SM Higgs boson search in the $\ell\nu b\bar{b}$ final state to discriminate between the non-SM signals and the backgrounds. In the case of the $\ell\ell b\bar{b}$ and $\nu\nu b\bar{b}$ analyses we select two regions with different signal purity. Events with $100 \leq m_{jj} \leq 150$ ($70 \leq m_{jj} \leq 150$) for $\ell\ell b\bar{b}$ ($\nu\nu b\bar{b}$) comprise the "high-purity" region (HP), while the rest of the events comprise the "low-purity" region (LP). In the $\ell\nu b\bar{b}$ case events with an MVA output less than 0 provide negligible sensitivity and are not considered further. The remaining events are split into two regions with different signal purity. The LP region consists of events with an MVA output less than 0.5, and the HP region consists of events with an MVA output greater than, or equal to, 0.5.

VI. CANDIDATE DISTRIBUTION

The number of contributing channels is large, and their sensitivity varies from one final state to another and with the event classification. The discriminating variables chosen and their binning are also not commensurate from one channel to another, and so the distributions cannot be simply summed. If the distributions were summed, then the channels with large backgrounds will dominate the sum and the signal will not be easily visible. To address these issues, we follow the procedure used in Ref [6] to visualize the aggregate data from the contributing channels. Bins with similar signal to background ratios (s/b) are summed together from all contributing sub-channels, and the data are displayed compared with the signal and background predictions. The distributions are shown separately for the 2^+ search and the 0^- search in Fig. 1. The backgrounds are fit to the data in each case, allowing the systematic uncertainties to float within their a priori constraints. For symmetry, neither the SM Higgs boson signal nor the exotic signal is included in these fits. The exotic signal, within the a priori constraints, is shown stacked, and the SM signal is shown as a separate, unstacked histogram. The sorting of the bins is performed using the ratio of the predicted exotic signal to the predicted background. Both signals are shown assuming $\mu_{\text{exotic}} = \mu_{\text{SM}} = 1$, where μ_{exotic} (μ_{SM}) is the scaling factor applied to the exotic (SM) Higgs boson signal. This representation of the data is not used to compute the final results, since the distribution indiscriminately sums unrelated backgrounds which are fit separately. It does, however, provide a guide to how much individual events contribute to the results and how well the signal is separated from backgrounds in the combined search. It furthermore illustrates the relative ability of the discriminating variables to distinguish between SM and exotic signals. Both distributions show agreement between the background predictions and the observed data over four orders of magnitude, and no evidence for an excess of exotic signal-like candidates.

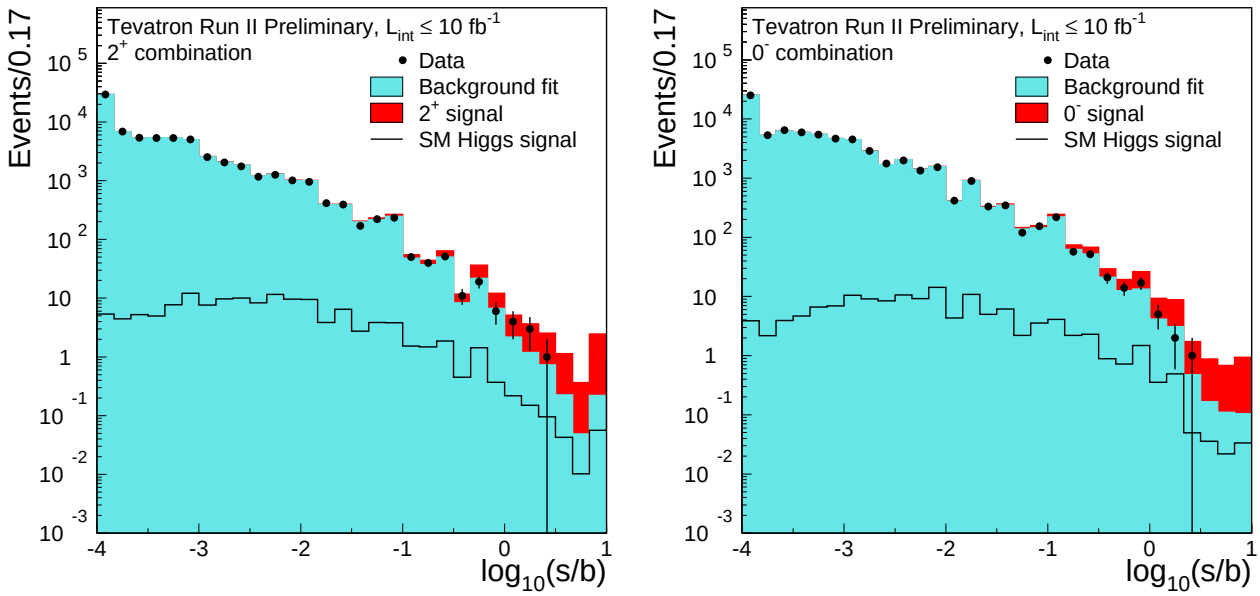

FIG. 1: Distribution of $\log_{10}(s/b)$, for the data from all contributing Higgs boson search channels from CDF and D0, for $m_H = 125$ GeV/c^2 for the 2^+ search (left-hand plot) and the 0^- search (right-hand plot). The data are shown with points, and the expected exotic signals are shown with $\mu_{\rm exotic} = 1$ stacked on top of the backgrounds, which are fit to the data within their systematic uncertainties. The s/b used to rank analysis bins is the exotic signal divided by the background. The background predictions do not include the contributions from the SM Higgs boson, which are shown as separate histograms, not stacked. The error bars shown on the data correspond in each bin to the square root of the observed data count. Underflows and overflows are collected into the leftmost and rightmost bins, respectively.

We also display in Fig. 2 the data distributions sorted by the ratio of the exotic signal to the predicted background, with the background subtracted. Wider bins are chosen than in Figure 1, and underflows and overflows are collected into the lowest and highest visible bins, respectively. As in Fig. 1, the background-only model has been fit to the data, allowing the systematic uncertainties to float. The signals are shown assuming $\mu_{\rm exotic} = \mu_{\rm SM} = 1$; the post-fit uncertainties on the background are also displayed. No excess of data is see above the background fits in the bins most sensitive to an exotic signal.

VII. COMBINING CHANNELS

To gain confidence that the final result does not depend on the details of the statistical formulation, we perform two types of combinations, using Bayesian and modified frequentist approaches. These two approaches were found to yield limits on the Higgs boson production rate that agree within 10% for all hypotheses tested, and within 1% on average for this result and previous works [6]. Both methods rely on distributions in the final discriminants, and not just on their single integrated values. Systematic uncertainties enter in the predicted number of signal and background events as well as on the distribution of the discriminants in each analysis ("shape uncertainties"). Both methods use likelihood calculations based on Poisson probabilities.

We interpret the results of the searches by computing exclusion limits, cross section fits, and p values for testing the 2^+ and 0^- hypotheses. The first step is the construction of a binned likelihood, combined for all contributing channels by multiplying the individual channels' likelihoods together. For a single channel, this likelihood is the product over all bins in the histogrammed final discriminant of the Poisson probability for observing the data in

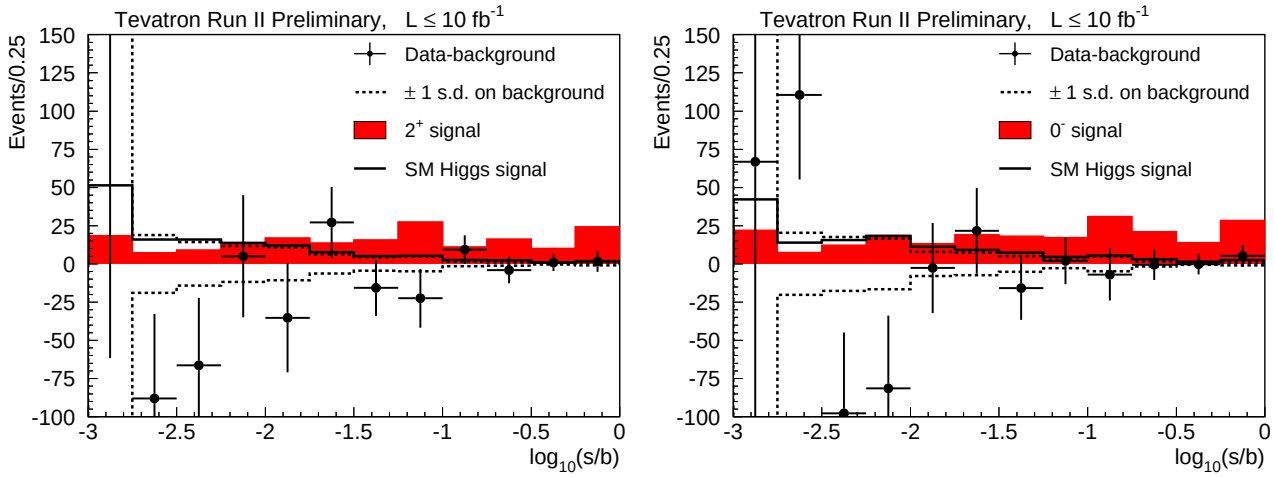

FIG. 2: Background-subtracted distribution of the discriminant histograms, summed for bins with similar signal-to-background ratio (s/b) over all contributing Higgs boson search channels from CDF and D0, for $m_H = 125$ GeV/c^2, for the 2^+ search (left-hand plot) and the 0^- search (right-hand plot). The background is fit to the data in each case, and the uncertainty on the background, shown with dashed lines, is after the fit. The exotic signal model, scaled to the SM Higgs boson expectation, is shown with a filled histogram. The SM Higgs boson expectation is also shown with a solid line. The error bars shown on the data points correspond in each bin to the square root of the sum of the expected signal and background yields. Underflows and overflows are collected into the leftmost and rightmost bins, respectively.

that bin given the signal and background predictions, as a function of the nuisance parameters, which express our systematic uncertainties. The joint likelihood takes the form

$$L(\text{data}|\mu_{\text{SM}}, \mu_{\text{exotic}}, \vec{s_{\text{SM}}}, \vec{s_{\text{exotic}}}, \vec{b}|\vec{n}, \vec{\theta}) \times \pi(\vec{\theta}) = \prod_{i=1}^{N_{\text{C}}} \prod_{j=1}^{N_{\text{bins}}} r_{ij}^{n_{ij}} \frac{e^{-r_{ij}}}{n_{ij}!} \times \prod_{k=1}^{n_{\text{sys}}} e^{-\theta_k^2/2}. \quad (1)$$

In this expression, the first product is over the number of channels (N_{C}), and the second product is over histogram bins containing n_{ij} events, binned in ranges of the final discriminant variables used for the individual analyses. The predictions for the bin contents are $r_{ij} = \mu_{\text{SM}} \times s_{\text{SM},ij}(\vec{\theta}) + \mu_{\text{exotic}} \times s_{\text{exotic},ij}(\vec{\theta}) + b_{ij}(\vec{\theta})$ for channel i and histogram bin j, where $s_{\text{SM},ij}$, $s_{\text{exotic},ij}$, and b_{ij} represent the expected SM Higgs boson signal, the exotic Higgs boson signal, and the SM background in the bin, respectively, and μ_{SM} (μ_{exotic}) is the scaling factor applied to the SM (exotic) Higgs boson signal as defined previously. By scaling all SM Higgs boson signal contributions by the same factor, we assume that the relative contributions of the different processes are as given by the SM. We also assume the SM production and decay ratios for the exotic Higgs boson, which is a mild assumption since all channels reported here are sensitive only to the $X \to b\bar{b}$ decay mode and the ratios of associated production with a W and a Z are likely to be close to those in the SM due to custodial symmetry.

Systematic uncertainties are parametrized by the dependence of $s_{\text{SM},ij}$, $s_{\text{exotic},ij}$, and b_{ij} on $\vec{\theta}$. Each of the n_{sys} components of $\vec{\theta}$, θ_k, corresponds to a single independent source of systematic uncertainty, and each parameter may have an impact on several sources of signal and background in different channels, thus accounting for correlations. Gaussian priors are assumed for the θ_k, truncated so that no prediction of any signal or background rate is negative.

To compute the exclusion limits and the best-fit cross sections, we adopt a Bayesian approach. In these calculations, the likelihood function, multiplied by the θ_k priors, $\pi(\theta_k)$, is then integrated over θ_k including correlations [53],

$$L'(\text{data}|\mu_{\text{SM}}, \mu_{\text{exotic}}) = \int L(\text{data}|\mu_{\text{SM}}, \mu_{\text{exotic}}, \vec{s}, \vec{b}|\vec{n}, \vec{\theta})\pi(\vec{\theta})d\vec{\theta}. \quad (2)$$

To compute upper limits on the rate of exotic Higgs boson production, we assume a uniform, non-negative prior in μ_{exotic} and obtain its posterior distribution. The observed 95% credibility upper limit on μ_{exotic}, $\mu_{\text{exotic},95^{\text{obs}}}$ is the

value of $\mu_{\rm exotic}$ such that the integral of the posterior density of $\mu_{\rm exotic}$ from zero to $\mu^{\rm obs}_{\rm exotic,95}$ corresponds to 95% of the integral of $\mu_{\rm exotic}$ from zero to infinity. The expected distribution of $\mu_{\rm exotic,95}$ is computed in an ensemble of pseudoexperiments generated without exotic signal. In each pseudoexperiment, random values of the nuisance parameters are drawn from their priors. The median expected value of $\mu_{\rm exotic,95}$ in this ensemble is denoted $\mu^{\rm exp}_{\rm exotic,95}$. The observed and expected upper limits on $\mu_{\rm exotic}$ are computed separately assuming the presence of a Higgs boson with SM properties, and also assuming its absence. The upper limits are listed in Table IV separately for 2^+ and 0^- bosons for the combined CDF and D0 searches.

We also perform two-dimensional cross section fits, allowing for the possibility of an arbitrary admixture of SM-like and exotic Higgs bosons. Assuming a uniform prior in the ($\mu_{\rm SM}$, $\mu_{\rm exotic}$) plane, we compute the posterior probability density for each of the input channels and their combination, separately for the 2^+ and 0^- exotic Higgs boson hypotheses. Figure 3 shows the two-dimensional domains integrating 68% and 95% of the posterior probability densities for the Tevatron combination. The point in the ($\mu_{\rm SM}$, $\mu_{\rm exotic}$) plane which maximizes the posterior probability density is shown as the best fit value. For the Tevatron combination, the best-fit values are ($\mu_{\rm SM}$=1.1, $\mu_{2^+}=0$) for the search for the 2^+ state, and ($\mu_{\rm SM}$=1.0, $\mu_{0^-}=0$) for the search for the 0^- state.

In the modified frequentist approach [54], we also compute p values for the discrete two-hypothesis tests, with the SM Higgs boson hypothesis on one hand, and the exotic hypothesis on the other. Because there are no theoretical predictions for the production cross sections and decay branching ratios for the exotic models, we choose to test the model ($\mu_{\rm SM}$=0, $\mu_{\rm exotic}$=1) against the model ($\mu_{\rm SM}$=1, $\mu_{\rm exotic}$=0). The test statistic used to compute these p values is the ratio of maximized likelihoods, shown here for the first case above, testing

$$\mathrm{LLR} = -2\ln\left(\frac{L(\mathrm{data}|\mu_{\rm SM}=0,\mu_{\rm exotic}=1,\hat{\theta})\pi(\hat{\theta})}{L(\mathrm{data}|\mu_{\rm SM}=1,\mu_{\rm exotic}=0,\hat{\hat{\theta}})\pi(\hat{\hat{\theta}})}\right) \tag{3}$$

where $\hat{\theta}$ are the best-fit values of the nuisance parameters assuming the exotic Higgs boson hypothesis, and $\hat{\hat{\theta}}$ are the best-fit values assuming the SM Higgs boson hypothesis. The LLR distributions for the combined CDF and D0 searches are shown in Fig. 4 for the 2^+ Higgs boson (left-hand plot), and the 0^- Higgs boson search (right-hand plot). The LLR distributions are shown separately assuming an exotic particle is present with $\mu_{\rm exotic}=1$ plus SM backgrounds, and if the SM Higgs boson plus SM backgrounds are present.

To compute the p values, pseudoexperiments are drawn either from the SM Higgs boson hypothesis or the exotic Higgs boson hypothesis, where values of the nuisance parameters are drawn randomly from their prior distributions. We compute two p values, which test either the SM hypothesis ($p_{\rm null}$) or the exotic hypothesis ($p_{\rm test}$). These are defined as

$$p_{\rm null} = P(\mathrm{LLR} \leq \mathrm{LLR}_{\rm obs}|\mathrm{SM}), \tag{4}$$

and

$$p_{\rm test} = P(\mathrm{LLR} \geq \mathrm{LLR}_{\rm obs}|\mathrm{exotic}). \tag{5}$$

We further define the values of $p_{\rm null}$ and $p_{\rm test}$ expected if the data agreed with the median LLR value for either the exotic model prediction or the SM prediction, respectively.

$$p^{\rm exotic}_{\rm null,med} = P(\mathrm{LLR} \leq \mathrm{LLR}^{\rm exotic}_{\rm med}|\mathrm{SM}), \tag{6}$$

and

$$p^{\rm SM}_{\rm test,med} = P(\mathrm{LLR} \geq \mathrm{LLR}^{\rm SM}_{\rm med}|\mathrm{exotic}). \tag{7}$$

A small value of $p_{\rm null}$ is the customary criterion for claiming evidence (with a threshold of 0.00135) or observation (with a threshold of 2.87×10^{-7}) of a new particle or process. A small value of $p_{\rm test}$ (typically 0.05) is used to exclude the test hypothesis. In order to prevent exclusion of models for which there is insufficient sensitivity, due to a downward fluctuation in the background, we also quote the values of

$$\mathrm{CL_s} = p_{\rm test}/(1-p_{\rm null}). \tag{8}$$

Table V lists the observed and the median expected values of $p_{\rm null}$, $p_{\rm test}$, and $\rm CL_s$ for the Tevatron combination, for the 2^+ and 0^- hypotheses, assuming $\mu_{\rm exotic}$=1. The median expected $p_{\rm null}$ values are computed assuming an exotic signal is present, and the median expected $p_{\rm test}$ and $\rm CL_s$ values are computed assuming the exotic signal is absent but a SM signal is present. In order to compute the very small values of $p_{\rm test}$ and the expected values of $p_{\rm null}$ and $p_{\rm test}$, the same approximation used by the ATLAS and CMS Collaborations, based on Wilks's theorem, is used [55]. Table V lists the p values and the equivalent number of Gaussian standard deviations z corresponding to each p value, using a one-sided definition

$$p = (1 - \mathrm{erf}(z/\sqrt{2}))/2. \tag{9}$$

A. Systematic Uncertainties

Systematic uncertainties differ between experiments and analyses, and they affect the rates and shapes of the predicted signal and background in correlated ways. The combined results incorporate the sensitivity of predictions to values of nuisance parameters, and include correlations between rates and shapes, between signals and backgrounds, and between channels within experiments and between experiments. More details on these issues can be found in the individual documents [6, 19, 20]. Here we consider only the largest contributions and correlations between and within the two experiments.

Sources of systematic uncertainty that affect both the normalization and the shape of the final discriminant distribution include jet energy scale (1–4)%, jet energy resolution (1–3)%, lepton identification, trigger efficiencies, and b-tagging. Uncertainties on lepton identification and trigger efficiencies range from 2% to 6% and are applied to both the signal and MC-based background predictions. These uncertainties are estimated from data-based methods separately by CDF and D0, and differ based on lepton flavor and identification category. The b-tagging efficiencies and mistag rates are similarly constrained by auxiliary data samples, such as inclusive jet data or $t\bar{t}$ events. The uncertainty on the per-jet b-tag efficiency is approximately 4%, and the mistag uncertainties vary between 7% and 15%.

The largest sources of uncertainty on the dominant backgrounds are the rates of V+heavy flavor jets, which are typically 20–30% of the predicted values. Using constraints from the data, the uncertainties on these rates are typically, a priori, 8% or less. The data samples in the V+jets selections prior to b-tagging are used as control samples to constrain systematic uncertainties in the MC modeling of the energies and angles of jets. Any residual discrepancy coming from the difference between light- and heavy-flavor components is shown to be smaller than the systematic uncertainties associated with the generator or the correction procedures themselves.

Significant sources of uncertainty for all analyses are the integrated luminosities used to normalize the expected signal yield and MC-based backgrounds, and the cross sections for the simulated backgrounds. The uncertainties on the measurements of the integrated luminosities are 6% (CDF) and 6.1% (D0). Of these values, 4% arises from the uncertainty on the inelastic $p\bar{p}$ scattering cross section, which is correlated between CDF and D0. CDF and D0 also share the assumed values and correlate uncertainties on the production cross sections for top-quark processes ($t\bar{t}$ and single top) and for electroweak processes (WW, WZ, and ZZ), using the values given earlier. Cross-section uncertainties of 6% and 7% are used for diboson and $t\bar{t}$ production respectively. The uncertainty on the expected multijet background in each channel is dominated by the statistics of the data sample from which it is estimated and varies from 10% to 30%.

VIII. SUMMARY

In summary, we have combined the CDF and D0 tests for a pseudoscalar Higgs boson with $J^P = 0^-$ and a graviton-like boson with $J^P = 2^+$ in the $WX \to \ell\nu b\bar{b}$, the $ZX \to \ell^+\ell^- b\bar{b}$, and the $ZX \to \not{E}_T b\bar{b}$ search channels using models described in [10]. No evidence is seen for either of the exotic particles, either in place of the SM Higgs boson or produced in a mixture with a $J^P = 0^+$ Higgs boson. The best-fit cross section times the decay branching ratio to $b\bar{b}$ is consistent with the prediction of the Standard Model Higgs boson.

TABLE IV: Observed and expected Bayesian upper limits on graviton-like (2^+) and pseudoscalar (0^-) Higgs boson production cross section times the decay branching ratio $Br(X \to b\bar{b})$, normalized to the SM prediction, assuming either that the SM Higgs boson (denoted SMH) is also present or absent.

Channel	obs (Limit/SM)	-2σ exp (Limit/SM)	-1σ exp (Limit/SM)	Median exp (Limit/SM)	$+1\sigma$ exp (Limit/SM)	$+2\sigma$ exp (Limit/SM)
2^+, No SMH Background	0.36	0.19	0.24	0.33	0.47	0.67
2^+, SMH Background	0.31	0.19	0.25	0.34	0.47	0.65
0^-, No SMH Background	0.36	0.17	0.23	0.32	0.45	0.64
0^-, SMH Background	0.29	0.18	0.23	0.32	0.45	0.62

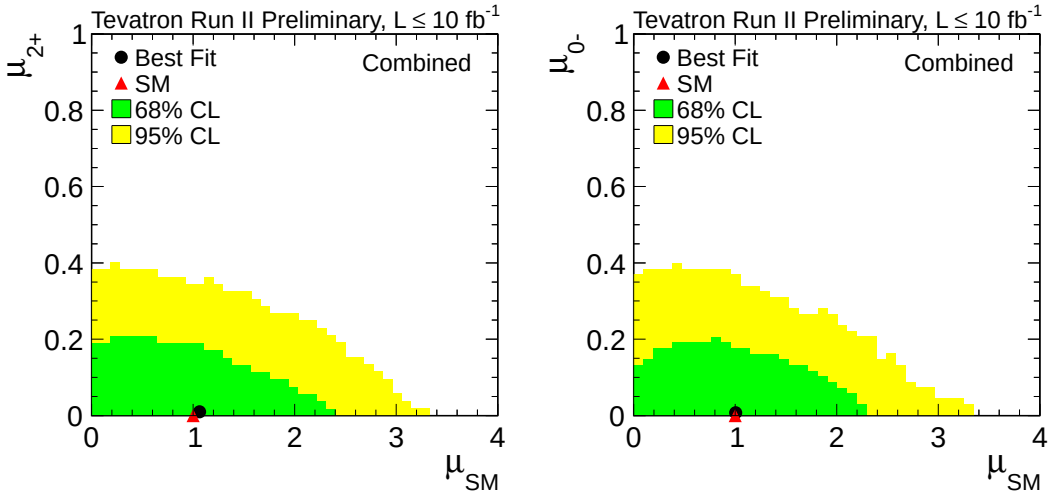

FIG. 3: Two-dimensional credibility regions in the (μ_{exotic},$\mu_{\rm SM}$), for the combination of CDF and D0's searches for the 2^+ Higgs boson (left-hand plot), and the 0^- Higgs boson (right-hand plot).

Upper limits at the 95% CL on the rate of the production of an exotic Higgs boson are set at 0.36 times the SM Higgs production rate for the 2^+ hypothesis, and 0.36 times the SM Higgs production rate for the 0^- hypothesis. If the production rate times the ($X \to b\bar{b}$) branching ratio of the exotic particle is the same as that predicted for the SM Higgs boson, then the exotic models are excluded with significances of 4.9 s.d. and 5.0 s.d. for the 2^+ and 0^- models, respectively.

Acknowledgments

We thank the Fermilab staff and technical staffs of the participating institutions for their vital contributions. We acknowledge support from the DOE and NSF (USA), ARC (Australia), CNPq, FAPERJ, FAPESP and FUNDUNESP (Brazil), NSERC (Canada), NSC, CAS and CNSF (China), Colciencias (Colombia), MSMT and GACR (Czech Republic), the Academy of Finland, CEA and CNRS/IN2P3 (France), BMBF and DFG (Germany), DAE and DST (India), SFI (Ireland), INFN (Italy), MEXT (Japan), the Korean World Class University Program and NRF (Korea), CONACyT (Mexico), FOM (Netherlands), MON, NRC KI and RFBR (Russia), the Slovak R&D Agency, the Ministerio de Ciencia e Innovación, and Programa Consolider-Ingenio 2010 (Spain), The Swedish Research Council (Sweden), SNSF (Switzerland), STFC and the Royal Society (United Kingdom), the A.P. Sloan Foundation (USA), and the EU community Marie Curie Fellowship contract 302103.

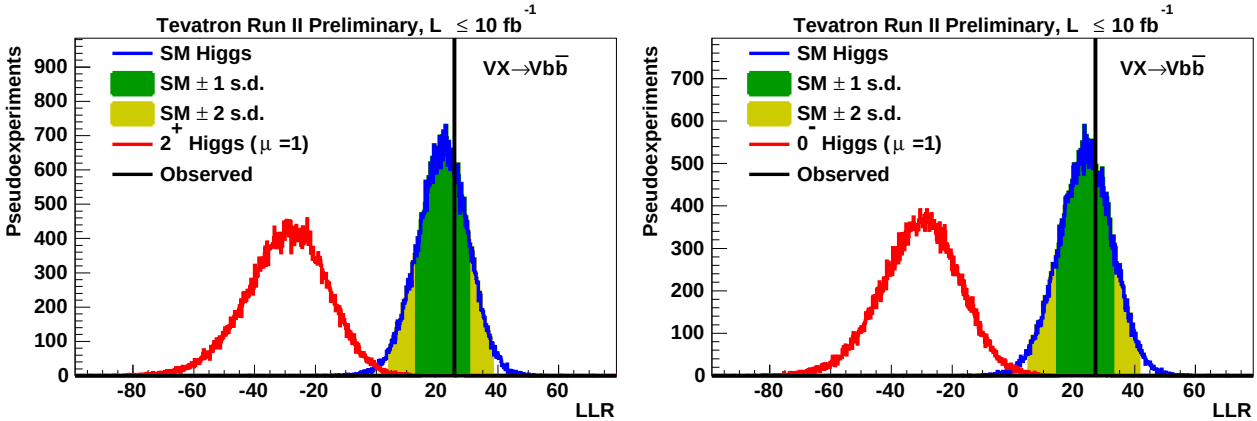

FIG. 4: Distributions of LLR in CDF and D0's combined searches for the 2^+ Higgs boson (left-hand plot), and the 0^- Higgs boson search (right-hand plot). The distributions of LLR are shown separately assuming an exotic particle is present with $\mu_{\rm exotic} = 1$ plus SM backgrounds, and if the SM Higgs boson plus SM backgrounds are present. The observed values of LLR are shown with vertical lines. Shaded regions show the 68% and 95% confidence level regions on the distributions assuming the SM Higgs boson is present, centered on the median expectation.

TABLE V: Observed and expected LLR values and p values for the combined CDF and D0 searches for the graviton-like (2^+) boson and the pseudoscalar (0^-) Higgs boson. Expected values are calculated using the median value of the relevant LLR distribution. The p values are listed directly and the corresponding significances in units of standard deviations using Equation 9 are listed in parentheses. For each exotic model tested, p values are reported both relative to the LLR value observed in data ($\mathrm{LLR_{obs}}$) and also relative to the median LLR values for the SM and exotic model.

Analysis	$J^P = 2^+$	$J^P = 0^-$
$\mathrm{LLR_{obs}}$	25.7	27.1
$\mathrm{LLR^{SM}_{med}}$	21.8	23.7
$\mathrm{LLR^{exotic}_{med}}$	-29.6	-29.9
$p_{\rm null}$	.66 (-0.41)	.63 (-0.34)
$p^{\rm exotic}_{\rm null,med}$	1.9×10^{-8} (5.5)	1.8×10^{-8} (5.5)
$p_{\rm test}$	1.9×10^{-7} (5.1)	9.4×10^{-8} (5.2)
$p^{\rm SM}_{\rm test,med}$	1.2×10^{-6} (4.7)	4.7×10^{-7} (4.9)
$\mathrm{CL_s}$	5.6×10^{-7} (4.9)	2.6×10^{-7} (5.0)
$\mathrm{CL^{SM}_{s,med}}$	2.3×10^{-6} (4.6)	9.4×10^{-7} (4.8)

[1] G. Aad *et al.* [ATLAS Collaboration], Phys. Lett. B **716**, 1 (2012).
[2] S. Chatrchyan *et al.* [CMS Collaboration], Phys. Lett. B **716**, 30 (2012)
[3] S. Chatrchyan *et al.* [CMS Collaboration], JHEP **1306**, 081 (2013).
[4] G. Aad *et al.* [ATLAS Collaboration], arXiv:1406.3827 [hep-ex].
[5] G. Aad *et al.* [ATLAS Collaboration], "Combined coupling measurements of the Higgs-like boson with the ATLAS detector using up to 25 fb^{-1} of proton-proton collision data" ATLAS-CONF-2013-034 (2013).
[6] T. Aaltonen *et al.* [CDF and D0 Collaborations], Phys. Rev. D **88**, 052014 (2013).
[7] G. Aad *et al.* [ATLAS Collaboration], "Study of the spin of the new boson with up to 25 fb^{-1} of ATLAS data, ATLAS-CONF-2013-040 (2013);
G. Aad *et al.* [ATLAS Collaboration], Phys. Lett. B **726**, 120 (2013).
[8] S. Chatrchyan *et al.* [CMS Collaboration], Phys. Rev. Lett. **110**, 081803 (2013);
S. Chatrchyan *et al.* [CMS Collaboration], J. High Energy Phys. **01**, 096 (2014).
[9] S. Chatrchyan *et al.* [CMS Collaboration], Phys. Rev. D **89**, 092007 (2014);
S. Chatrchyan *et al.* [CMS Collaboration], Submitted to Eur. Phys. J. C. arXiv:1407.6369 [hep-ex].
[10] J. Ellis, D. S. Hwang, V. Sanz and T. You, JHEP **1211**, 134 (2012) [arXiv:1208.6002 [hep-ph]].
[11] D. J. Miller, S. Y. Choi, B. Eberle, M. M. Mühlleitner and P. M. Zerwas, Phys. Lett. B **505**, 149 (2001) [hep-ph/0102023].
[12] T. Aaltonen *et al.* [CDF and D0 Collaborations], Phys. Rev. Lett. **109**, 071804 (2012) [arXiv:1207.6436 [hep-ex]].
[13] S. Chatrchyan *et al.* [CMS Collaboration], *Nature Physics* **10**, 557 (2014).
[14] G. Aad *et al.* [ATLAS Collaboration], "Evidence for Higgs Boson Decays to the $\tau^+\tau^-$ Final State with the ATLAS Detector", ATLAS-CONF-2013-108 (2013).
[15] S. Chatrchyan *et al.* [CMS Collaboration], JHEP **05**, 104 (2014).
[16] G. Aad *et al.* [ATLAS Collaboration], "Search for the bb decay of the Standard Model Higgs boson in associated (W/Z)H production with the ATLAS detector", ATLAS-CONF-2013-079 (2013).
[17] S. Chatrchyan *et al.* [CMS Collaboration], "Search for the standard model Higgs boson produced in association with a W or a Z boson and decaying to bottom quarks", arXiv:1310.3687v2.
[18] J. Ellis and V. Sanz, private communication.
[19] CDF Collaboration, "Tests of the Spin and Parity of the Higgs Boson with CDF", CDF Note 11103 (2014).
[20] D0 Collaboration, "Constraints on models of the Higgs boson with exotic spin and parity in $VH \to Vb\bar{b}$ final states", To appear in Phys. Rev. Lett. arXiv:1407.6369 [hep-ex].
[21] V. M. Abazov *et al.* [D0 Collaboration], Phys. Rev. D **88**, 052008 (2013).
[22] V. M. Abazov *et al.* [D0 Collaboration], Phys. Lett. B **716**, 285 (2012).
[23] V. M. Abazov *et al.* [D0 Collaboration], Phys. Rev. D **88**, 052010 (2013).
[24] V. M. Abazov *et al.*, [D0 Collaboration], Nucl. Instrum. Meth Phys. Res. A. **763**, 290 (2014).
[25] V. M. Abazov *et al.* [D0 Collaboration], Nucl. Instrum. Meth. Phys. Res. A **620**, 490 (2010).
[26] J. Freeman, T. Junk, M. Kirby, Y. Oksuzian, T. J. Phillips, F. D. Snider, M. Trovato and J. Vizan *et al.*, Nucl. Instrum. Meth. A **697**, 64 (2013).
[27] T. Sjöstrand, L. Lonnblad and S. Mrenna, "PYTHIA 6.2: Physics and manual," arXiv:hep-ph/0108264.
[28] M. L. Mangano, M. Moretti, F. Piccinini, R. Pittau and A. D. Polosa, "ALPGEN, a generator for hard multiparton processes in hadronic collisions," JHEP **0307**, 001 (2003).
[29] S. Frixione and B.R. Webber, JHEP **0206**, 029 (2002).
[30] G. Corcella *et al.*, JHEP **0101**, 010 (2001).
[31] A. Pukhov *et al.*, "CompHEP: A package for evaluation of Feynman diagrams and integration over multi-particle phase space. User's manual for version 33," [arXiv:hep-ph/9908288].
[32] J. M. Campbell and R. K. Ellis, Phys. Rev. D **60**, 113006 (1999).
[33] U. Langenfeld, S. Moch, and P. Uwer, Phys. Rev. D **80**, 054009 (2009).
[34] T. Aaltonen *et al.* [CDF and D0 Collaborations], Phys. Rev. D **86**, 092003 (2012).
[35] A. D. Martin, W. J. Stirling, R. S. Thorne and G. Watt, Eur. Phys. J. C **63**, 189 (2009).
[36] N. Kidonakis, Phys. Rev. D **74**, 114012 (2006).
[37] R. Hamberg, W. L. van Neerven, and T. Matsuura, Nucl. Phys. **B359**, 343 (1991) [Erratum-ibid. **B644**, 403 (2002)].
[38] J. Baglio and A. Djouadi, arXiv:1003.4266 [hep-ph] (2010). We have obtained extended versions of the table of WH and ZH cross sections for all Higgs boson masses we test, and with more digits of precision, from the authors.
[39] The Fortran program can be found on Michael Spira's web page `http://people.web.psi.ch/~mspira/proglist.html`.
[40] O. Brein, A. Djouadi, and R. Harlander, Phys. Lett. B **579**, 149 (2004).
[41] M. L. Ciccolini, S. Dittmaier, and M. Kramer, Phys. Rev. D **68**, 073003 (2003).

[42] H. L. Lai *et al.*, Phys. Rev D **55**, 1280 (1997).
[43] J. Alwall, M. Herquet, F. Maltoni, O. Mattelaer, and T. Stelzer, J. High Energy Phys. **06**, 128 (2011).
[44] S. Dittmaier *et al.* [LHC Higgs Cross Section Working Group Collaboration], [arXiv:1101.0593 [hep-ph]].
[45] S. Dittmaier, S. Dittmaier, C. Mariotti, G. Passarino, R. Tanaka, S. Alekhin, J. Alwall and E. A. Bagnaschi *et al.*, Distributions," arXiv:1201.3084 [hep-ph].
[46] A. Djouadi, J. Kalinowski and M. Spira, Comput. Phys. Commun. **108**, 56 (1998).
[47] A. Bredenstein, A. Denner, S. Dittmaier, and M. M. Weber, Phys. Rev. D **74**, 013004 (2006);
A. Bredenstein, A. Denner, S. Dittmaier, and M. Weber, JHEP **0702**, 080 (2007);
A. Bredenstein, A. Denner, S. Dittmaier, A. Mück, and M. M. Weber, JHEP **0702**, 080 (2007) `http://omnibus.uni-freiburg.de/~sd565/programs/prophycey4f/prophecy4f.html` (2010).
[48] J. Baglio and A. Djouadi, JHEP **1103**, 055 (2011).
[49] A. Denner, S. Heinemeyer, I. Puljak, D. Rebuzzi, and M. Spira, Eur. Phys. J. C **71**, 1753 (2011).
[50] T. Aaltonen *et al.* [CDF Collaboration], Phys. Rev. Lett. **109**, 111804 (2012).
[51] T. Aaltonen *et al.* [CDF Collaboration], Phys. Rev. D **87**, 052008 (2013).
[52] T. Aaltonen *et al.* [CDF Collaboration], Phys. Rev. Lett. **109**, 111803 (2012).
[53] T. Junk, Nucl. Instrum. Meth. A **434**, 435 (1999);
A.L. Read, "Modified Frequentist analysis of search results (the CL_s method)", in F. James, L. Lyons and Y. Perrin (eds.), *Workshop on Confidence Limits*, CERN, Yellow Report 2000-005, available through `cdsweb.cern.ch`.
[54] W. Fisher, "Systematics and Limit Calculations," FERMILAB-TM-2386-E.
[55] ATLAS and CMS Collaborations, "Procedure for the LHC Higgs boson search combination in Summer 2011," ATLAS-PHYS-PUB-2011-011, CMS NOTE-2011/005 (2011).